Investigations of Trailing Edge Stall on 2D Airfoils

Karen Mulleners, Arne Henning, Markus Raffel

Institute for Aerodynamics and Flow Technology, German Aerospace Centre, Göttingen, Germany,
karen.mulleners@dlr.de, arne.henning@dlr.de, markus.raffel@dlr.de

Abstract A combined approach of time resolved particle image velocimetry and a proper orthogonal decomposition (POD) method is adopted to investigate the complex topological structure of the flow separating from an airfoil at large angle of attack. The application of global time resolved imaging of the trailing edge separation region yields significant insight into the formation and evolution of large-scale vortical structures. The topological structure of the separated flow over an airfoil depends on the type of stall. Trailing edge stall in a supercritical flow regime is associated with the formation of a laminar separation bubble, i.e. a localized region of laminar separation, transition and reattachment, followed by separation of the turbulent boundary layer at the trailing edge. The wake region is characterized by alternately shedding of counter rotating vortices as a result of the interaction between the shear layer due to the separating boundary layer and the shear layer instability that develops at the trailing edge. Measurements have been carried out in the wake of a NACA 4415 airfoil section at high angle of attack. The ensemble of PIV snapshots has been analysed using a proper orthogonal decomposition method in order to identify and characterize coherent structures.

1. Introduction

The flow structure behind a bluff body in general depends on the state of the boundary layer and the location of the laminar to turbulent transition. According to the nomenclature of Schewe (2001) a flow regime is called subcritical when a laminar boundary layer is separating and laminar to turbulent transition occurs in the separated boundary layer. The turbulent boundary does not reattach in contrary to the supercritical regime where reattachment leads to the formation of a separation bubble. The supercritical flow is characterized by turbulent separation and a narrower wake region.

An airfoil at large angle of attack can be considered as bluff body. The topological structure of flow separation from an airfoil in the subcritical and the supercritical flow regime is illustrated in Fig. 1. Flow separation from an airfoil under supercritical conditions is referred to as trailing edge stall.

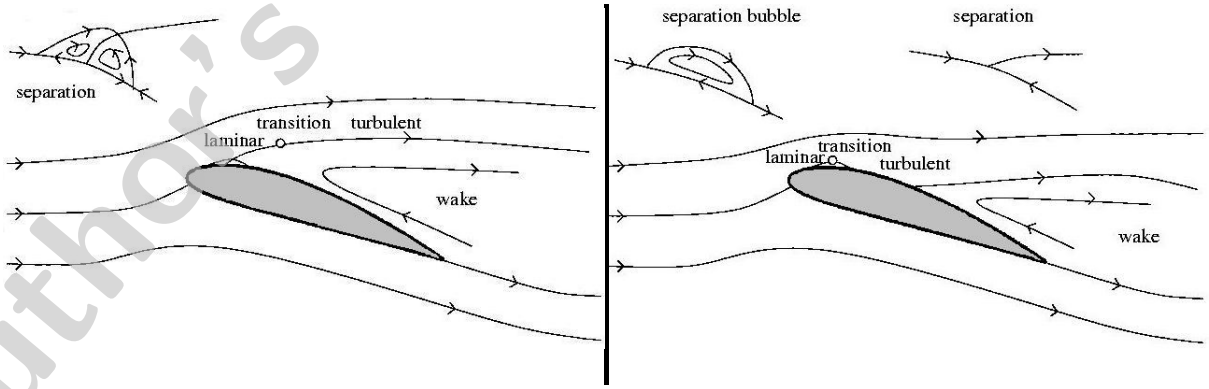

Fig. 1 Schematic representation of the flow separating from an airfoil in the subcritical flow regime (*left*) and the supercritical flow regime (*right*) (Kindler 2004)

The separation region consists of three fundamental ingredients: the shear layer due to the separating boundary layer, the shear layer at the trailing edge and the wake flow. Interaction of the shear layers causes the wake to become unstable. Due to the presence of a relatively large backflow region the wake is far from being slender, hence the formation of vortical structures is not a result of a free shear layer instability, like the Kelvin-Helmholtz instability, but is expected to be analogue to the formation of large-scale structures in the wake of a circular cylinder at supercritical Reynolds numbers.

This paper presents the investigation of the complex flow system in the wake of a trailing edge separation of an NACA 4415 airfoil section at large angle of attack. The formation and temporal evolution of coherent structures, as well as characteristic length scales and frequencies are analyzed by means of time resolved particle image velocimetry measurements and a proper orthogonal decomposition (POD) method which is attributed to Lumley (1970). The essential features of the flow topology are discussed, focusing on the formation and evolution of large-scale structures. The vortex shedding phenomenon is further characterized by means of the coefficients resulting from the POD analysis.

2. Proper orthogonal decomposition

The basic idea of the proper orthogonal decomposition (POD), also known as the Karhunen-Loeve expansion, applied to a non-homogeneous velocity field, is to determine a set of orthogonal functions or eigenmodes, with random coefficients that represent the field as good as possible based on an energy-weighted measure. The eigenmodes are sorted in descending order with respect to their energy content with the dominant eigenmodes representing the characteristic features of the flow.

The implementation of the POD is based on the method of snapshots (Sirovich, 1987), providing a decomposition of the velocity field $f(x)$

$$f_n(x) = \sum_{n=1}^{N} a_n \psi_n(x) \tag{1}$$

where $f_n(x) = f(x, \mathrm{n}\tau)$ is an instantaneous flow field or snapshot and N the total number of snapshots. The time scale τ is the reciprocal of the PIV sampling frequency. Since the eigenmodes $\psi_n(x)$ are orthonormal, the respective mode coefficients a_n are uncorrelated

$$\langle a_n a_m \rangle = \lambda_n \delta_{nm} . \tag{2}$$

Here the operator $\langle \ldots \rangle$ denotes ensemble averaging. The eigenvalue λ_n represents the contribution of the corresponding eigenmode $\psi_n(x)$ to the total energy of the field. According to Sirovich (1987) the eigenmodes have the form

$$\psi(x) = \sum_{n=1}^{N} \zeta_n f_n(x) \tag{3}$$

where the coefficients ζ_n are determined by the eigenfunctions of the spatial correlation matrix C given by the inner product of the velocity fields at times n and m

$$C_{nm} = \frac{1}{N}\left(f_n, f_m\right). \tag{4}$$

Note that POD defines a mathematical framework and the association of the eigenfunctions of the correlation operator with coherent structures is based on interpretation and fluid dynamical intuition.

3. Experimental set-up

Measurements have been performed in the closed-circuit, continuous low-speed wind tunnel at DLR Göttingen. The wind tunnel has an open test section with a rectangular nozzle (0.7 m x 1.0 m). Free stream velocities up to 50 m/s can be reached.
The airfoil model was a NACA 4415 profile with a chord length *c* of 200 mm and an aspect ratio Æ of 4 which was enclosed between two circular end plates with a diameter of 400 mm in order to reduce finite span effects. The angle of attack was fixed at $\alpha = 20°$. Two component time resolved particle image velocimetry measurements have been conducted in the cross sectional plane at model mid-span for two different free stream velocities, U_∞ = {20 m/s, 25 m/s} with respective Reynolds numbers $Re = \{2.5\times10^5, 3.1\times10^5\}$.
The TR-PIV system consisted of a frequency doubled Nd:YAG laser, which supports Q-switch frequencies up to 30 kHz and a pair of CMOS cameras with a 1024 x 1024 pixel sensor, capable of operating at 3000 fps at full resolution. Series of 3072 PIV image frame pairs have been taken with an acquisition rate of 1.5 kHz (3000 fps), corresponding to a measurement time of approximately 2s. The images were recorded using frame-straddling, where the time delay τ between the light pulses was 90 μs at U_∞ = 20 m/s and 70 μs at U_∞ = 25 m/s. The cameras were mounted side by side so that the cameras' fields of view covered the airfoil's trailing edge and wake (see Fig. 2).
The spatial resolution for both fields of view was 7.0 px/mm. The PIV images were processed using an interrogation window size of 16 px × 16 px and a 50% overlap yielding a grid spacing of 8 px or 1.14 mm.

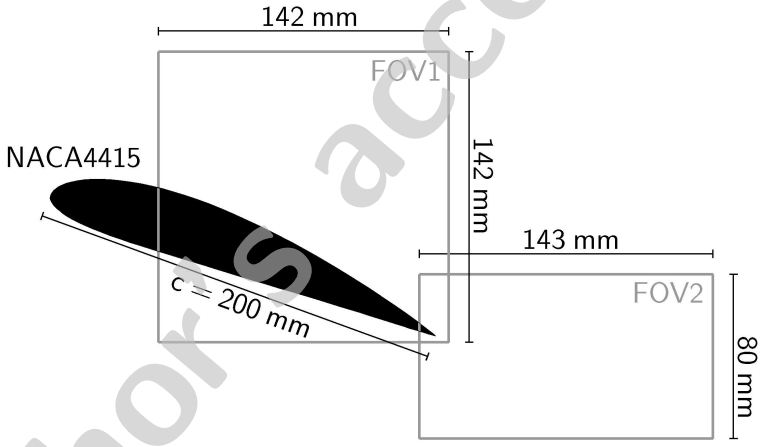

Fig. 2 Location of the camera FOVs

4. Results

The flow regime is found to be supercritical, i.e. the state of the boundary layer at separation is turbulent. The wake of the airfoil is narrower than in case of a subcritical state where the laminar to turbulent transition takes place in the separating boundary layer and the turbulent boundary layer does not reattaches. Characteristic features of the flow in the wake of the turbulent separation will be discussed below, focusing on the formation and convection of large-scale structures.

4.1 Flow topology

Figure 3 represents the measured two-component velocity vector field of two instantaneous flow fields, under the same experimental conditions at $Re = 3.1\times10^5$. Every second vector is shown and an offset vector, in form of the free stream flow vector, has been subtracted in order for vortical structures to be easily identified.

At approximately 70% chord length the flow separates and a large backflow region is formed resulting in the development of shear layers at the interface of the backflow region and the free stream flow. The shear layer due to the separating boundary layer is unstable and small-scale vortical structures, Kelvin-Helmholtz vortices, can be identified in both images. Additionally, Fig. 4 presents a close up view of the respective top shear layer instabilities and demonstrates the spatial resolution of the PIV measurements. In these plots all velocity vectors are shown, i.e. the distance between individual vectors is 1.14 mm.

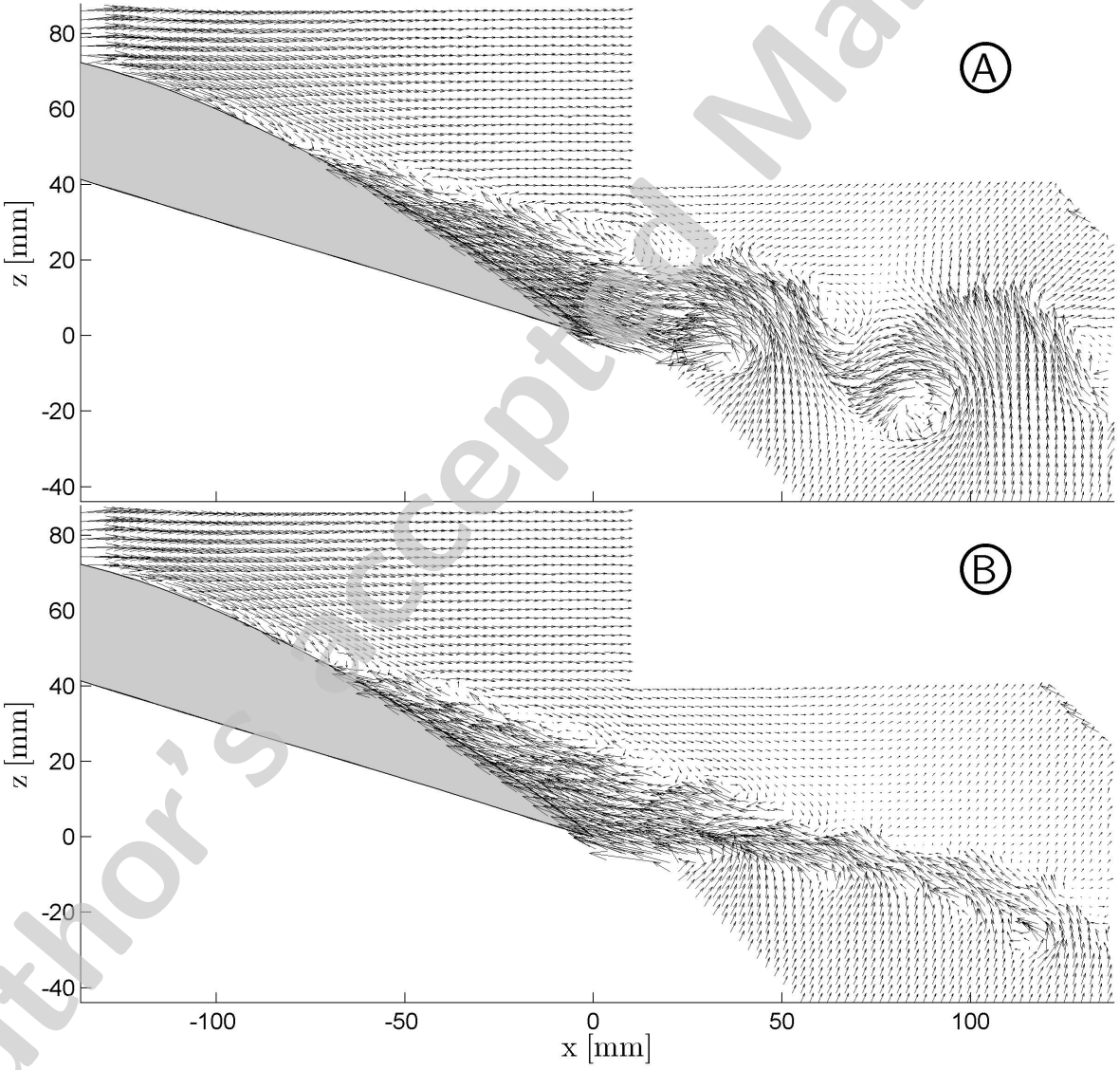

Fig. 3 Flow fields of two PIV snapshots at $Re = 3.1\times10^5$; small-scale vortical structures in the shear layer leading to a absolute instability and the formation of large-scale Kármán like vortices (*top*) and a convective instability (*bottom*)

Downstream the separation point towards the airfoil's trailing edge there are no fundamental differences between the flow fields represented by the top and bottom images in Fig. 3, which are labeled as type **A** and type **B**, respectively. The distinguishing feature of the type **A** flow field is the presence of large-scale Kármán-like vortices in the near wake. The pattern of vortical structures in the near wake can not be thought of as free flow instability, i.e. Kelvin-Helmholtz instability, but is equivalent to the von Kármán vortex street in the wake of a circular cylinder at supercritical Reynolds numbers. The counter rotating vortices are alternately shed as a result of the interaction between the shear layers that enclose the backflow region. The separated flow develops a global oscillation and the large-scale vortical structures are convected downstream. This is illustrated by a series of snapshots of vorticity contours in the left column of Fig. 5. The vorticity is scaled with the ratio of free stream velocity and airfoil chord length. The time increment between successive images is the reciprocal of the acquisition rate of the PIV recording, $\Delta t = 0.67$ ms.

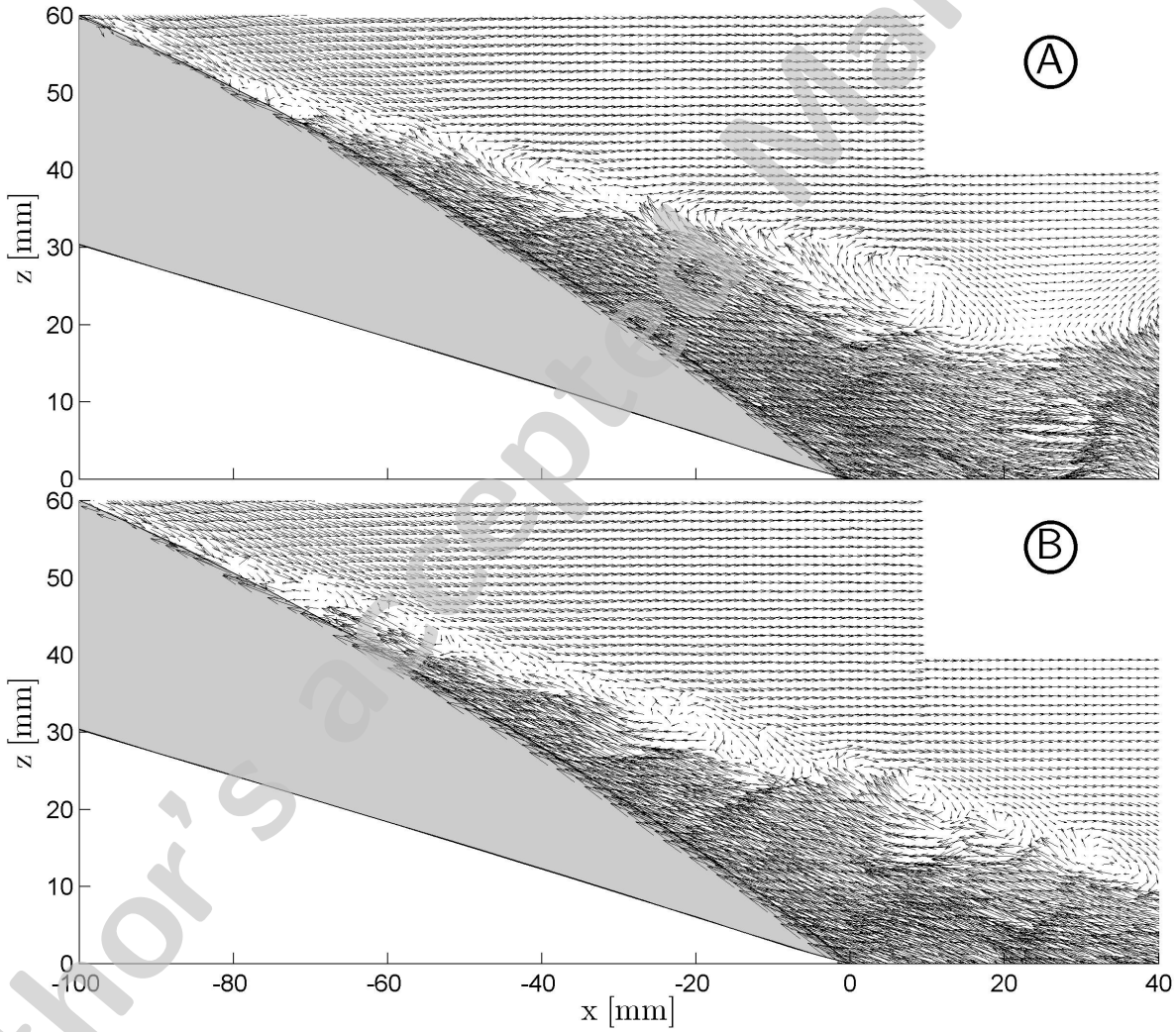

Fig. 4 Close-up view of the small-scale shear layer vortices or Kelvin-Helmholtz vortices of the two snapshots in Fig. 2

Analogously, the images in the right column of Fig. 5 illustrate the vorticity concentrations for subsequent snapshots corresponding to the type **B** flow. In contrast to the wake of type **A** flow, the type **B** wake is not oscillating and layers of positive and negative vorticity are arranged on top of each other. Apparently the unsteady separated flow is convectively unstable and small coherent

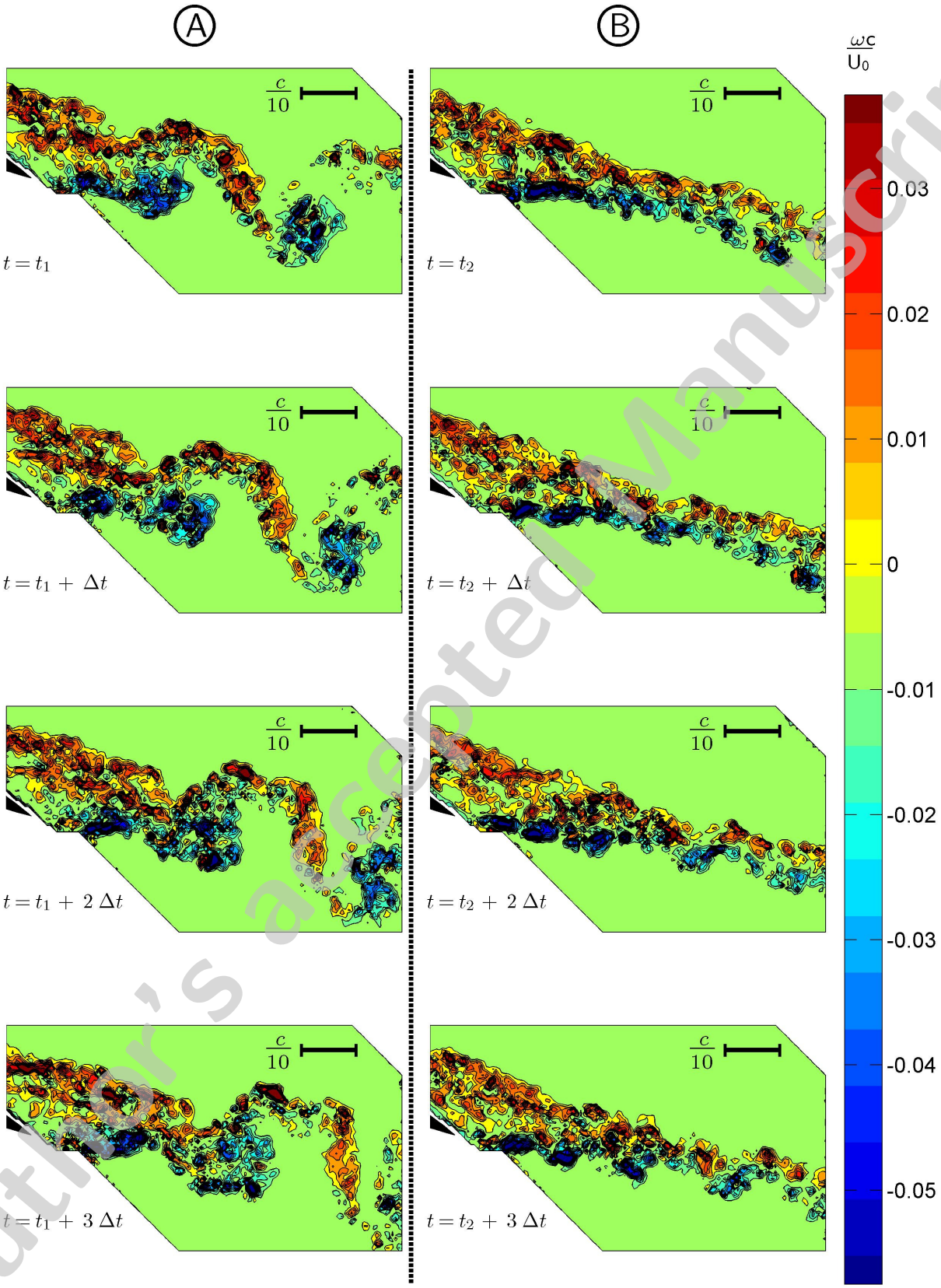

Fig. 5 Successive snapshots of vorticity contours of type **A** flow fields representing a absolute instability (*left*) and of type **B** flow fields representing a convective instability (*right*); ($Re = 3.1\times10^5$, $\Delta t = 0.67$ ms)

structures are convected downstream without being spatially amplified. A comprehensive review concerning absolute and convective instabilities is given by Huerre and Monkewitz (1990). From a practical perspective, type **B** flows are interesting because due to the absence of large-scale vortex shedding less energy is dissipated in the turbulent wake which in turn implies drag reduction. However convectively unstable flows are very sensitive to small perturbations and these states are not persistent. During the measurement the flow constantly switches between state **A** and **B**.

4.2 POD analysis

Proper orthogonal decomposition (POD) is applied in order to identify and characterize coherent structures in the type **A** wake flow. The implementation of the POD is based on the method of snapshots and the ensemble of PIV snapshots associated with the camera field of view in the wake (FOV2 in Fig. 2) is analyzed. Assuming the large-scale vortical structures to account for the main content of turbulent kinetic energy, the fluctuating velocity fields are considered. Moreover, only the vertical components are used which seem to be more pertinent for the identification of coherent structures in the airfoil's wake, since the boundaries of the coherent patterns are smeared when including the stream-wise velocity fluctuations.
The POD analysis yields a number of eigenmodes and eigenvalues equal to the number of snapshots included. The eigenmodes are sorted in descending order with respect to their relative contribution to the total energy of the fluctuating vertical motion, given by the respective eigenvalues. The distribution of the first 20 eigenvalues for the two measurement conditions, $Re = 2.5\times10^5$ and $Re = 3.1\times10^5$ is presented in Fig. 6.

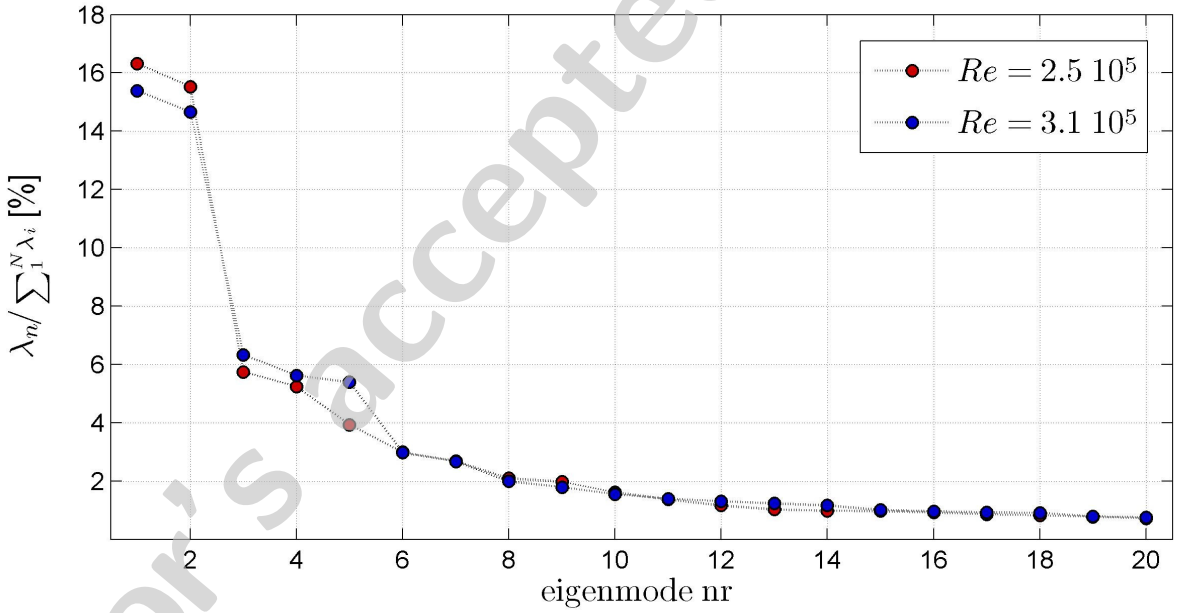

Fig. 6 Relative contribution of the first 20 eigenmodes to the total energy of the fluctuating vertical motion

The first issue observation is the elevation of the first two eigenvalues, pointing at the dominance of the first two modes. Together they contain more than 30% of the total energy of the fluctuating vertical motion in the wake. The successive eigenvalues and thus the energy content of the successive eigenmodes rapidly drops. Furthermore if two subsequent eigenvalues are nearly equal and the respective modes are complementary, these modes are coupled and form a mode pair.
The first four normalized POD eigenmodes for $Re = 3.1\times10^5$ are depicted in Fig. 7 by means of filled contour plots. The first two modes present a similar pattern, which is consistent with the

acknowledgement of them being a mode pair. The pattern, consisting of a succession of large-scale spatial structures with alternating sign, is spatially shifted by a quarter wavelength in the second mode with respect to the first. The effect of superimposing both modes is to introduce the convection of the flow pattern they present.

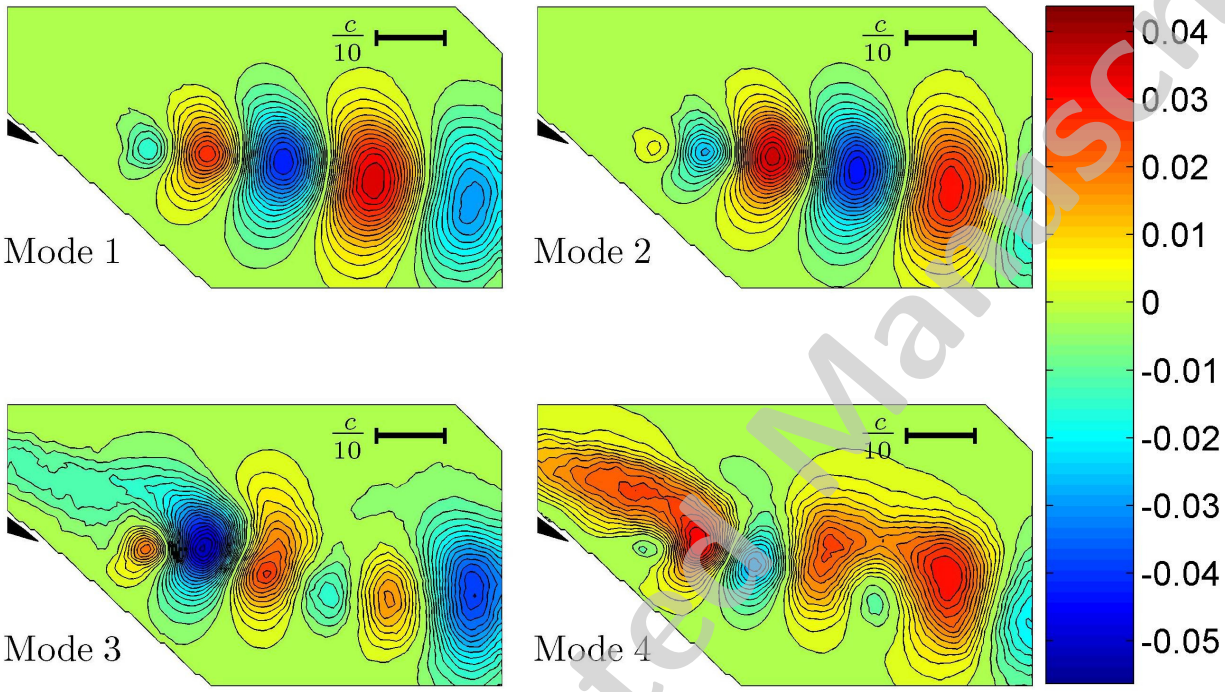

Fig. 7 First four normalized eigenmodes of the fluctuating vertical flow field for $Re = 3.1\times10^5$

4.3 Characterization of vortex shedding using POD coefficients

The observations made in the previous paragraph suggest that the dynamics of dominant periodic vortex shedding can be described by a low order flow model, i.e. a reconstruction of the flow field incorporating only the first two POD modes:

$$w'_{LOM}(x) = a_1\psi_1(x) + a_2\psi_2(x). \tag{5}$$

The subscript LOM denotes low order model and (a_1, a_2) are the mode coefficients associated with the first two modes, determined from the projection on the POD modes according to Eq. 1. Since the modes are an orthonormal set, the coefficients a_i are normalized by $\sqrt{2\lambda_i}$ (Eq. 2).
Furthermore if f_0 is the frequency of the dominant vortex shedding, the vortex shedding phase angle φ is a linear function of time, corresponding to $\varphi = 2\pi f_0 t$, and the evolution of the mode coefficients is given by

$$\begin{aligned} a_1(\varphi) &= \sqrt{2\lambda_1}\cos(\varphi) \\ a_2(\varphi) &= \sqrt{2\lambda_2}\sin(\varphi) \end{aligned}. \tag{6}$$

The distribution of the low order mode coefficients a_1 and a_2 of all instantaneous field realizations

for $Re = 3.1\times10^5$ is represented in Fig. 8 (*left*). In the ideal case of a coherent motion in absence of higher order harmonics as well as random turbulent fluctuations, the points in the normalized coefficient plane $\left(a_1/\sqrt{2\lambda_1}, a_2/\sqrt{2\lambda_2}\right)$ physically describe a circle (Ben Chiekh et al. 2004). However, for the experimental case presented here, the coefficients plotted in Fig. 8 (*left*) seem to cover an entire disk area.

The mode coefficients are a measure of the relative energy contribution of the corresponding mode, hence small values for both a_1 and a_2 indicate absence of large-scale vortical structures. Consequently the concentration of points in the center of the theoretical curve imply type **B** flow field.

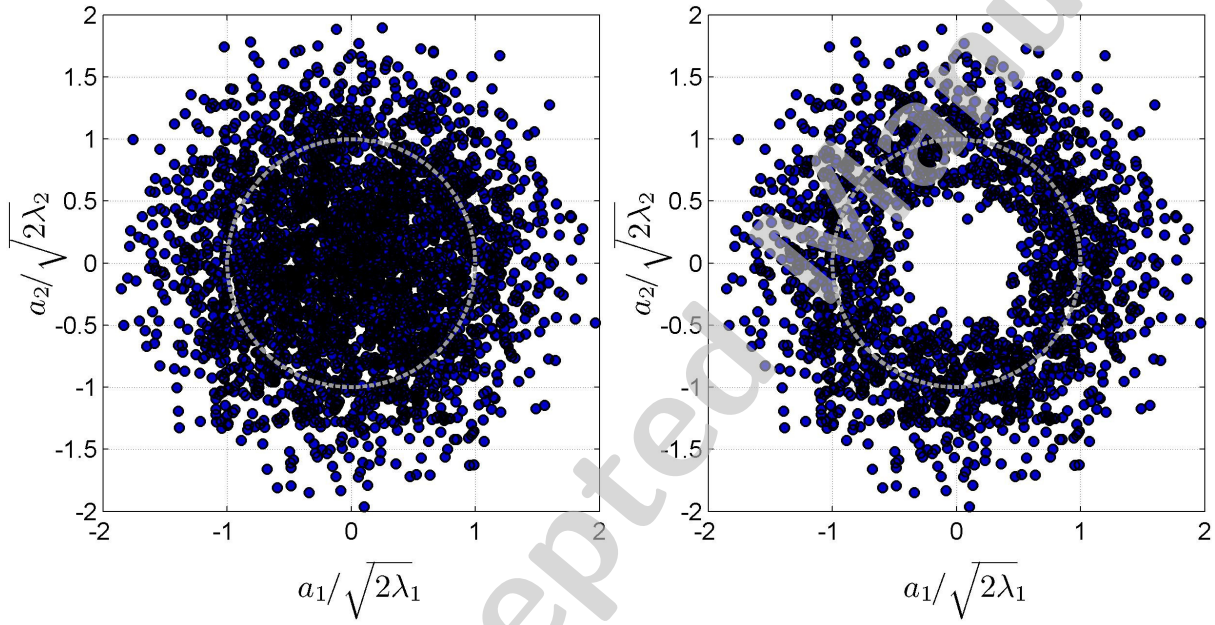

Fig. 8 Distribution of the mode coefficients of order *1* and *2* ($Re = 3.1\times10^5$); for the ensemble of field realizations (*left*), for the field realizations representing dominant vortex shedding (*right*)

One method to distinguish distinctly between flow types could be to define a threshold value respective to the radius of the circle in the coefficient plane that draws the boundary between type **A** and type **B**. A drawback of this approach is that the threshold value would have to be chosen arbitrarily.

Therefore another procedure is used here. The distinguishing feature of a type **A** flow field is the presence of large-scale coherent structures in the near wake. Hence the dominance of the first mode pair should be evident from the decomposition of the flow field according to eq. 1, meaning that the maximum of the series $|a_i(t_n)|$ is expected to be a_1 or a_2. For every single snapshot the maximum mode coefficient has been calculated. Almost 70% of the field realizations have a maximum for a_1 or a_2 and are classified as type **A** flow fields. The classification allows for investigation of the vortex shedding process based on type **A** flow fields only.

The distribution of the mode coefficients a_1 and a_2 confined to snapshots representing dominant vortex shedding is presented in Fig. 8 (*right*). The data points are more or less located around a circle, and the scatter around the theoretical curve can be explained as due to cycle-to-cycle variations of the vortex shedding process, induced by small scale fluctuations or turbulence. Moreover, the data points describe the circle in chronological order with an approximately constant frequency, which is linked to the propagation or convection speed of the flow pattern described by the linear combination of the dominant mode pair (ψ_1, ψ_2).

Hence, the coefficients of the linear combination represent the relative phases of the corresponding eigenmodes and the dominant frequency of the periodic vortex shedding can be found by a frequency analysis of the time evolution of a_1 and a_2. The power spectra of the whole signals and of the 'filtered' signals, i.e. confined to coefficients respective to type **A** flow fields, are presented in Fig. 9. When considering a strong, regular vortex shedding regime, such as the von Kármán vortex street behind a circular cylinder at low Reynolds numbers, discrete power spectra are expected with one or several fundamental components and their harmonics. The spectra respective the measurements on the other hand are broadened, which implies that the formation of large-scale structures is weak and irregular, as already indicated by the dispersion of the data points in the coefficient plane (Fig. 8 on the *right*). This is analogue to the vortex shedding in the wake of a circular cylinder at supercritical Reynolds numbers. The Strouhal number for a circular cylinder based on the cylinder diameter, $St = fd/U_\infty$, in the supercritical regime varies from 0.15 to 0.7 (Roshko 1960). For the experiments a Strouhal number has been calculated based on the wake width. Estimating the wake width at 0.04 m yield St ≈ 0.6 - 0.5, for $Re = 2.5\times10^5$ and $Re = 3.1\times10^5$ respectively. This is a satisfactory result.

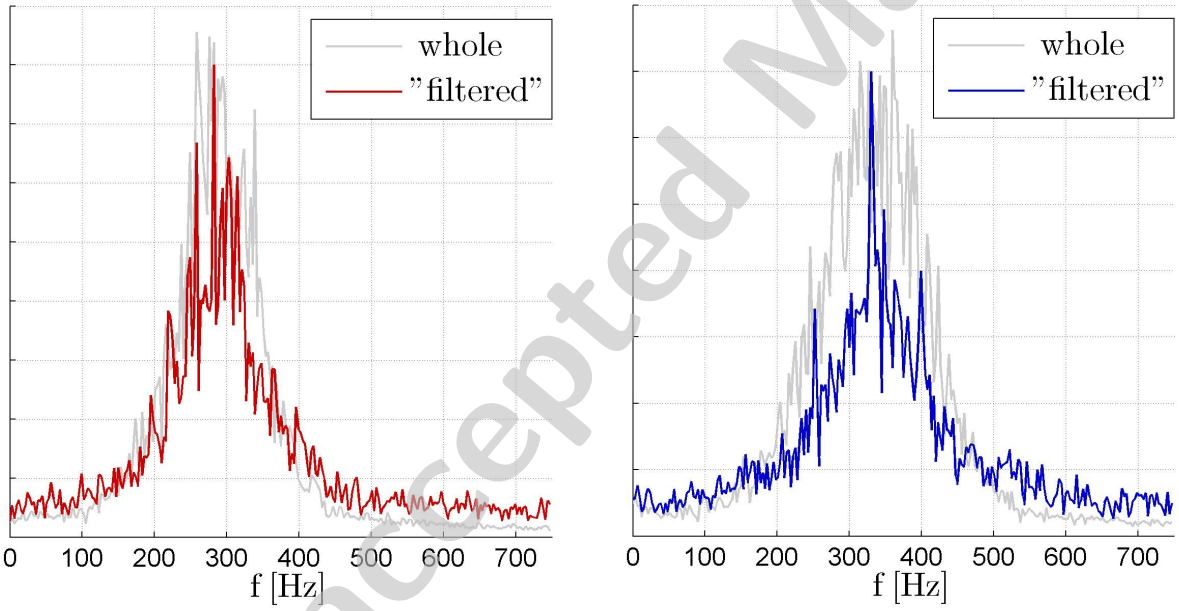

Fig. 9 Power spectrum of the first mode coefficient, $a_1(t)$; (——) whole signal, (——/——) 'filtered' signal; $Re = 2.5\times10^5$ (*left*), $Re = 3.1\times10^5$ (*right*)

However, this does not explain yet why the flow field in some snapshots shows no large-scale structures at all. Measurements are performed in a vertical plane at the model mid-span and only the in-plane velocity components have been measured. The PIV snapshots thus give a two-dimensional representation whereas the flow under the chosen experimental conditions is expected to be highly three-dimensional (Williamson 1996). Lateral motion of organized three-dimensional structures alters the view in the measurement cross section and vortex shedding might still be present but at shifted spanwise position.

On the other hand, intensive studies on vortex shedding from bluff bodies with the aid of hydrodynamic instability theory have given significant insight into this issue (Huerre and Monkewitz 1990; Oertel 1990). Interaction between small-scale vortical structures in the shear layer causes the flow in the near wake to become absolutely unstable and consequently yields the formation of large-scale Kármán-like vortices. Small disturbances of the shear layer vortices has strong influence on the flow characteristics in the near wake and consequently on the conditions for

which the flow becomes absolutely unstable. This offers the possibility of wake control. Several measures that affect vortex shedding in the wake of a bluff body are described by Schumm (1994). Density variations in the wake for example are found to be effective in suppression of vortex shedding. Perhaps the absence of large-scale structures in the wake is an effect of wake heating due to laser illumination.
Another possibility for the underlying mechanism is related to the coupling of the laminar separation bubble and trailing edge separation. The intrinsic motion of the separation bubble causes small-scale structures to emerge in the separating boundary layer leading to fluctuations of the trailing edge separation point. This in turn could yield variation in local stability properties.

5. Conclusion and perspectives

Time-resolved PIV recordings of the flow separating from an airfoil at large angle of attack have been submitted to a POD analysis in order to study the complex topological structure of the flow. It revealed the existence of vortex shedding as a coherent phenomenon superimposed on the turbulent wake flow. The dynamics of the dominant periodic vortex shedding has been described by a low order flow model. The global time resolved imaging of the trailing edge wake region yielded insight into the phenomenon of vortex shedding. The formation of large-scale vortical structures has been found to be irregular, analogously to the vortex shedding in the wake of a circular cylinder at supercritical Reynolds numbers.
Furthermore it has been noticed that the flow field in some snapshots shows no large-scale structures at all. The underlying mechanism is still unclear but three dimensional effects seem to be most likely.
This issue will be the further addressed in of future experiments. Simultaneous PIV measurements in the wake and instationary pressure measurements on the airfoil's surface will be conducted in order to investigate the correlation between vortex formation in the wake and fluctuations of separation bubble location. High spatial resolution measurements in the region of the separating shear layer should given more clarity about the interaction of the small-scale vortices.
Furthermore, similar measurements are planned in the wake of an oscillating airfoil aiming at studying the influence of the oscillation frequency on the vortex shedding process and the role of a dynamic stall vortex.

References

Ben Chiekh M, Michard M, Grosjean N, Béra JC (2004) Reconstruction temporelle d'un champ aérodymnamique instationnaire à partir de mesure PIV non résolues dans le temps. In 9ième Congrès Francophone de Vélocimétrie Laser, 14-17th September, Brussels, Belgium

Huerre P, Monkewitz P (1990) Local and global instabilities in spatially developing flows. Ann Rev Fluid Mech 22:473

Kindler K, Kreplin H, Ronneberger D (2004) Coherent structures in critical wing flows. In 12th international symposium on applications of laser techniques to fluid mechanics, 12-15th July, Lisbon, Portugal

Lumley J (1970) Stochastic tools in turbulence. Academic Press, New York, NY.

Oertel H, Jr (1990) Wakes behind bluff bodies. Ann Rev Fluid Mech 22:539

Schewe G (2001) Reynolds number effect in flow around more or less bluff bodies. J Wind Eng Ind Aerod 89:1267

Schumm M, Berger E, Monkewitz P (1994) Self-excited oscillations in the wake of two-dimensional bluff bodies and their control. J Fluid Mech 271:17

Sirovich L (1987) Turbulence and the dynamics of coherent structures; part I - III. Quart of Appl Math 45(3):561

Williamson C (1996) Vortex dynamics in the cylinder wake. Ann Rev Fluid Mech 28:477